Supporting information for:

Brown carbon in fine particles in four typical cities in Northwest China during wintertime: coupling optical properties with chemical processes

Miao Zhong[a,b], Jianzhong Xu[a,*], Huiqin Wang[c], Li Gao[d], Haixia Zhu[e], Lixiang

Zhai[a,b], Xinghua Zhang[a], Wenhui Zhao[a,b]

[a]State Key Laboratory of Cryospheric Sciences, Northwest Institute of Eco-Environment and

Resources, Chinese Academy of Sciences, Lanzhou 730000, China

[b]University of Chinese Academy of Sciences, Beijing 100049, China

[c]Institute of Desert Meteorology, China Meteorological Administration, Urumqi 830002, China

[d]School of Geography and Planning, Ningxia University, Yinchuan 750021, China

[e]Key Laboratory of Comprehensive and Highly Efficient Utilization of Salt Lake Resources, Qinghai

Institute of Salt Lakes, Chinese Academy of Science, Xining, Qinghai 810008, China

Corresponding to: Jianzhong Xu (jzxu@lzb.ac.cn)

Table S1. The daily average concentrations of $PM_{2.5}$, SO_2, NO_2, CO, O_3, T, and RH in YC, XN, UR and LZ during sampling time (Data from air quality database in China).

Sampling Site	Sample ID	Sampling Date	$PM_{2.5}$ ($\mu g/m^3$)	SO_2 ($\mu g/m^3$)	NO_2 ($\mu g/m^3$)	CO (mg/m^3)	O_3 ($\mu g/m^3$)
YC	1	12/6/2019	77	26	74	2	81
	2	12/9/2019	26	9	32	0.7	92
	3	12/12/2019	63	35	63	2.2	62
	4	12/16/2019	59	10	45	1.2	50
	5	12/19/2019	104	14	50	1.1	65
	6	12/23/2019	79	31	55	1.8	62
	7	12/26/2019	16	10	31	0.6	83
	8	12/30/2019	37	27	40	1.3	62
	9	1/2/2020	118	68	77	3.5	34
	10	1/6/2020	123	18	55	2.1	42
	11	1/9/2020	213	29	75	3	57
	12	1/13/2020	79	8	51	1.3	72
	13	1/16/2020	93	10	47	1.4	61
	14	1/20/2020	39	18	42	0.9	73
XN	15	12/5/2019	51	31	54	1.7	74
	16	12/9/2019	37	24	53	1.7	76
	17	12/12/2019	59	34	50	2.1	39
	18	12/16/2019	54	16	52	1.3	60
	19	12/19/2019	57	14	56	2.1	88
	20	12/23/2019	42	31	54	2	77
	21	12/26/2019	47	16	45	1.3	70
	22	12/30/2019	37	26	48	1.6	77
	23	1/2/2020	85	32	66	2.3	75
	24	1/7/2020	38	13	54	2.2	90
	25	1/9/2020	57	11	43	1.1	100
	26	1/13/2020	69	21	46	1.5	93
	27	1/16/2020	89	17	47	2	79
	28	1/20/2020	78	21	43	1.6	100
Sampling Site	Sample ID	Sampling Date	$PM_{2.5}$ ($\mu g/m^3$)	SO_2 ($\mu g/m^3$)	NO_2 ($\mu g/m^3$)	CO (mg/m^3)	O_3 ($\mu g/m^3$)

	29	12/5/2019	156	12	86	2.6	49
	30	12/9/2019	169	4	70	2.1	29
	31	12/12/2019	151	5	66	3.1	19
	32	12/16/2019	65	3	42	1.3	36
	33	12/19/2019	57	5	42	1.2	23
	34	12/23/2019	55	6	42	1.1	49
	35	12/26/2019	82	7	55	2.1	25
	36	12/30/2019	137	8	61	2.2	38
	37	1/2/2020	111	8	71	2.2	29
UR	38	1/6/2020	186	6	87	2.6	24
	39	1/9/2020	178	8	90	2.9	17
	40	1/13/2020	148	8	63	2.3	56
	41	1/16/2020	142	7	54	1.8	53
	42	1/20/2020	106	9	52	1.4	78
	43	12/5/2019	97	34	102	2.5	35
	44	12/10/2019	88	49	86	2.8	46
	45	12/13/2019	87	50	92	2.8	34
	46	12/16/2019	35	19	44	0.8	66
	47	12/20/2019	70	34	84	2	48
	48	12/23/2019	78	57	88	3.1	28
	49	12/26/2019	85	30	60	1.7	36
LZ	50	12/30/2019	57	44	75	1.9	39
	51	1/2/2020	65	26	80	2.2	21
	52	1/6/2020	81	11	57	0.8	68
	53	1/11/2020	63	16	68	1.4	72
	54	1/13/2020	50	20	65	1.2	56
	55	1/16/2020	85	20	72	1.9	52
	56	1/20/2020	59	29	76	2.2	54

Table S2. The excitation and emission wavelengths at the maximum fluorescence intensity of each PARAFAC component.

PARAFAC	Ex (nm)	Em (nm)	Component	References
C1	230/320	375	LO-HULIS	(Li et al., 2021)
C2	215/255	364	-	(Tang et al., 2020)
C3	240/325	414	HO-HULIS	(Chen et al., 2020)
C4	225/275	338	Protein-like	(Chen et al., 2020)
C5	210/280	373	LO-HULIS	(Chen et al., 2020; Chen et al., 2021)
C6	220	292	phenol-like	(Barsotti et al., 2016; Yan and Kim, 2017; Chen et al., 2020)

Table S3. Pearson's correlation coefficients calculated through the correlation analysis between water-soluble inorganic ions and WSOC. The bold highlighting the correlation was significant (at the level of 0.05).

r	YC	XN	UR	LZ
Na^+	-0.02	0.36	0.49	0.01
NH_4^+	**0.87**	**0.56**	**0.73**	**0.87**
K^+	**0.77**	**0.78**	**0.54**	**0.76**
Ca^{2+}	-0.01	0.11	0.33	0.39
Mg^{2+}	0.20	0.43	0.30	0.41
Cl^-	**0.79**	0.45	**0.87**	**0.75**
NO_3^-	**0.84**	0.50	**0.67**	**0.63**
SO_4^{2-}	**0.91**	0.49	**0.73**	**0.85**

Table S4. Summary of the multiple linear regression results based on four WSOA factors, and regression coefficients B (m^2/g) represent the fitted MAE value of each WSOA factor.

	coefficients	
	B (m^2/g)	Standard Error
LO-OOA	1.34	0.08
WS-POA	1.33	0.08
HO-OOA1	1.10	0.12
HO-OOA2	0.58	0.09
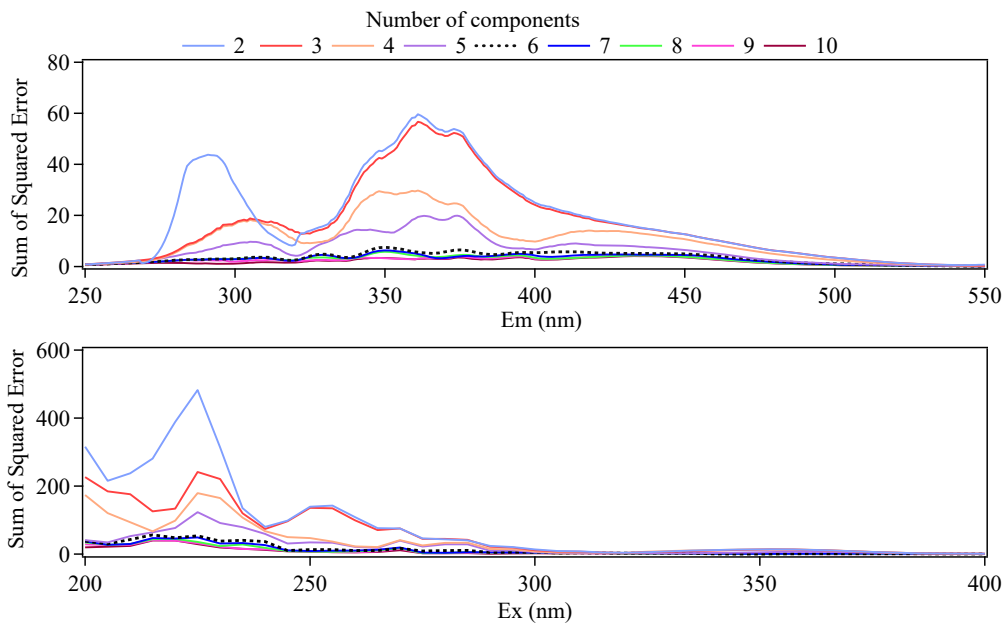
Figure S1. Sum of squared error of excitation and emission wavelength for 2–10 PARAFAC model. The bold black dotted line (C6) indicates the number of factors selected in this work.
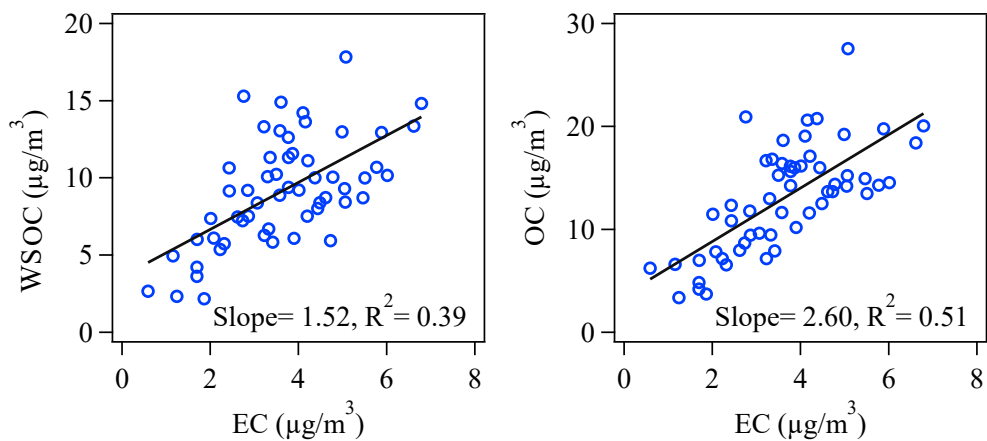
Figure S2. Scatter plots of WSOC, OC versus EC for four cities samples.
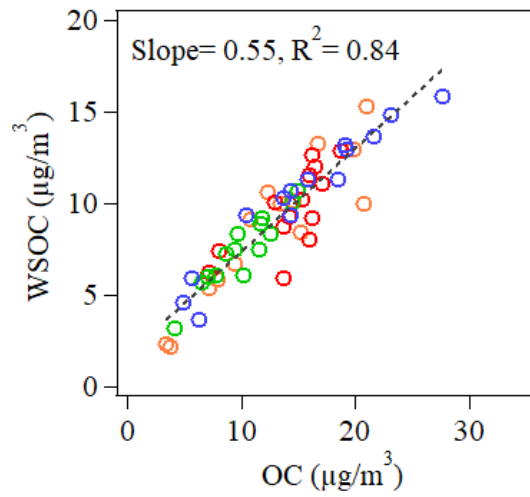
Figure S3. Scatter plots of WSOC versus OC for four cities samples.
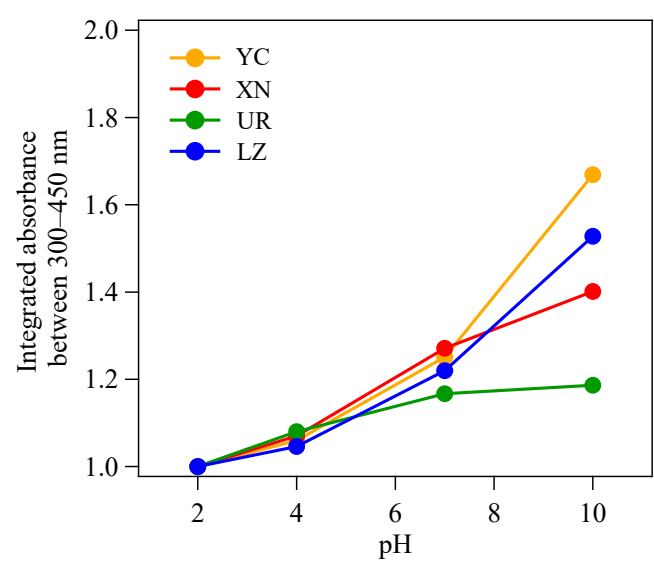
Figure S4. Integrated absorbance (300−450 nm) normalized to values at pH 2 as a function of pH for YC (orange), XN (red), UR (green), and LZ (blue) samples.
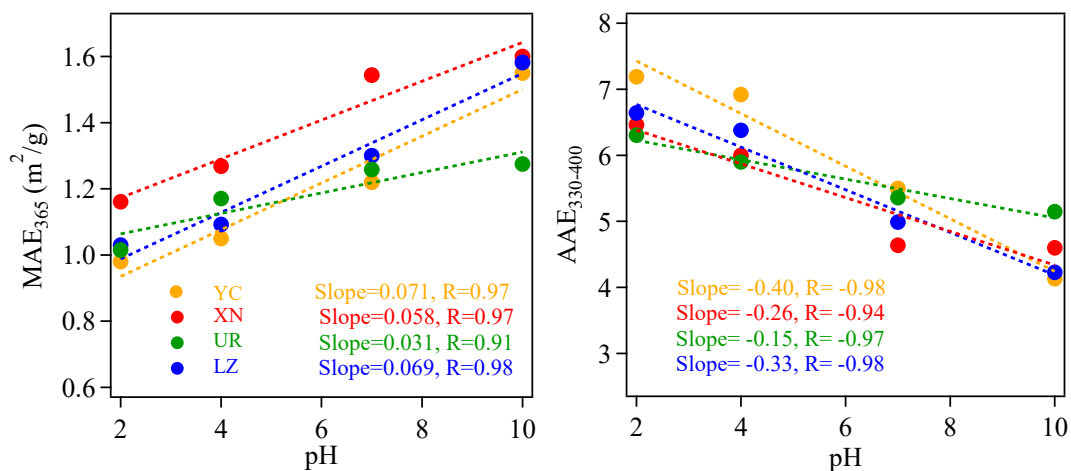
Figure S5. (a) MAE$_{365}$ and (b) AAE as a function of pH for YC (orange), XN (red), UR (green), and LZ (blue) samples.
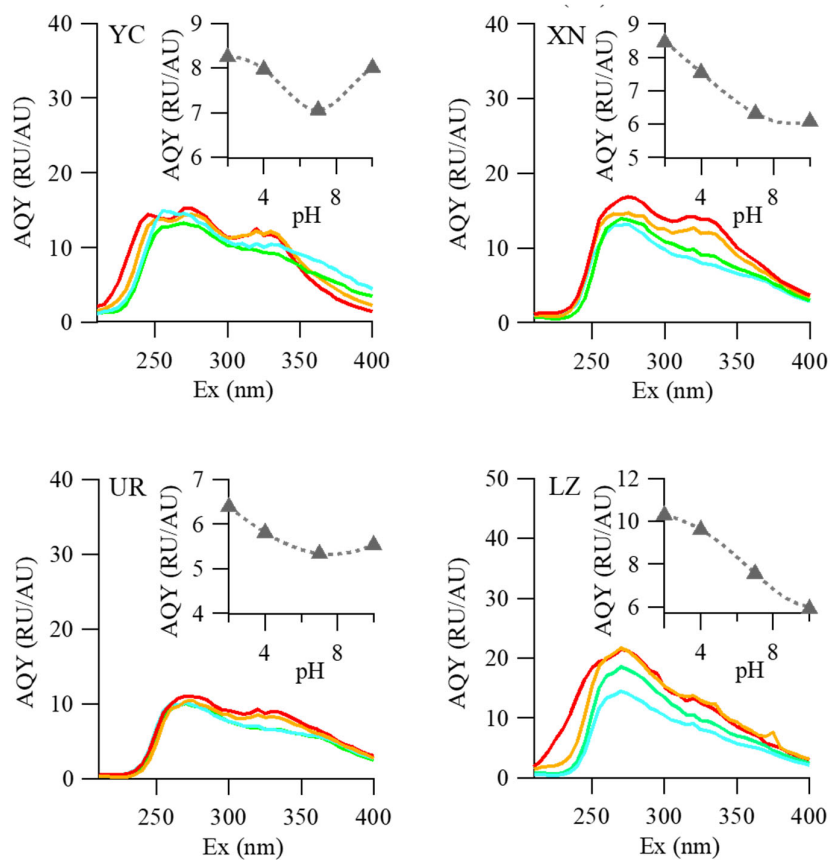
Figure S6. AQY against the excitation wavelength at different pH values. The insert figure shows the average AQY over all excitation wavelengths at different pH.
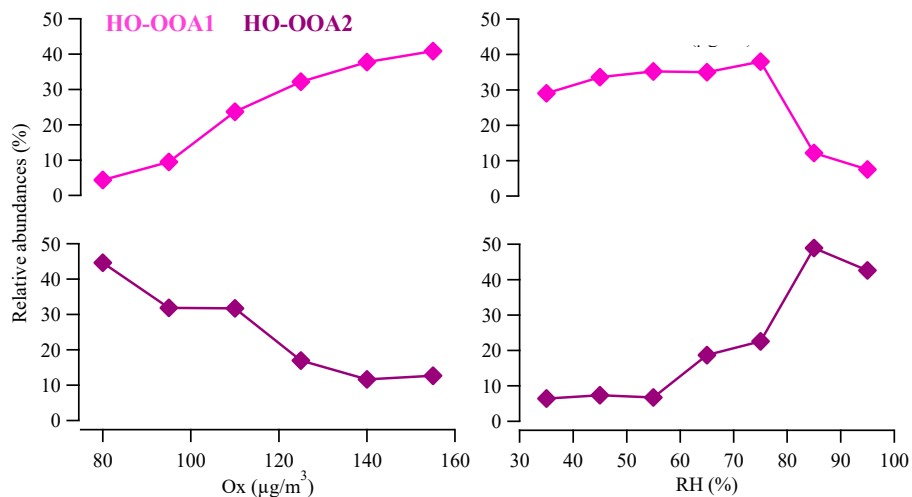
Figure S7. The mass contribution of HO-OOA1 and HO-OOA2 varied with odd oxygen ($O_x = O_3 + NO_2$) and RH. Note that O_x was averaged at 15 $\mu g/m^3$ intervals and RH was averaged at 10% intervals.
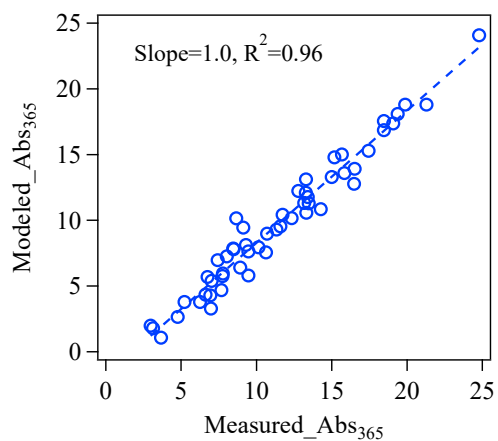
Figure S8. Scatter plot of modeling Abs_{365} using multiple linear regression (MLR) analysis versus measured Abs_{365} for WSOA in four cities.
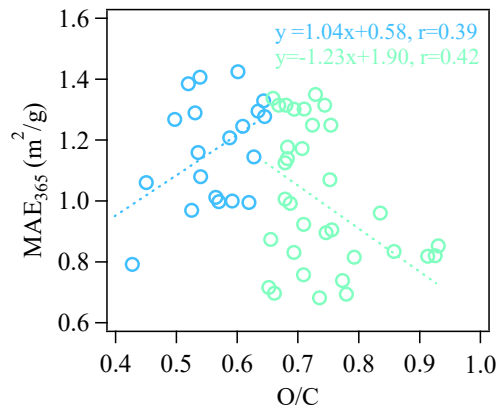
Figure S9. MAE$_{365}$ as a function of O/C ratio. O/C critical value of 0.64 was selected to divide all samples into two groups (blue and green circles), each group is fitted by least-squares linear regression, and the correlation was significant at the level of 0.05.
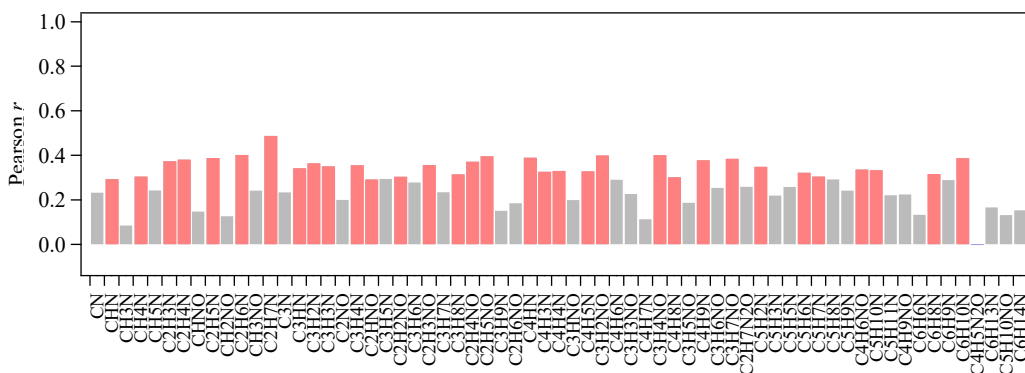
Figure S10. Pearson's correlation coefficients calculated through the correlation analysis between the mass concentration of the N-containing fragments and the light absorption coefficient of WSOA. The red bars highlighting the correlation was significant (at the level of 0.05).
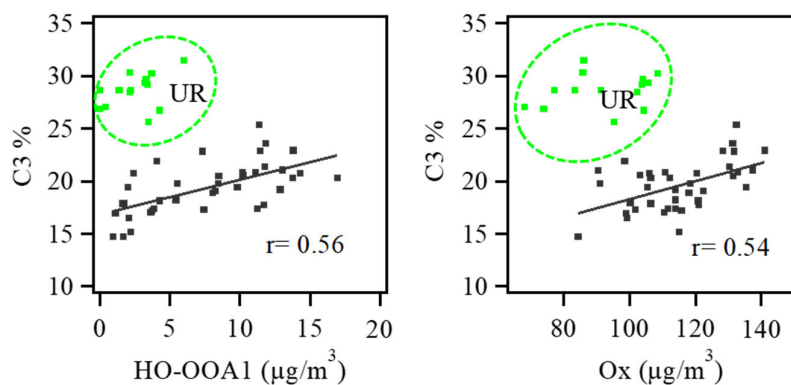
Figure S11. Scatter plots of the relative contents of C3 versus the mass concentration of HO-OOA1 factors and odd oxygen (O$_x$ = O$_3$ + NO$_2$) for four cities samples. Significant positive correlations observed when UR data (green dots) were excluded.

References

Barsotti, F., Ghigo, G., and Vione, D.: Computational assessment of the fluorescence emission of phenol oligomers: A possible insight into the fluorescence properties of humic-like substances (HULIS), J. Photochem. Photobiol. A Chem., 315, 87-93, https://doi.org/10.1016/j.jphotochem.2015.09.012, 2016.

Chen, Q., Hua, X., Li, J., Chang, T., and Wang, Y.: Diurnal evolutions and sources of water-soluble chromophoric aerosols over Xi'an during haze event, in Northwest China, Sci. Total Environ., 786, 147412, https://doi.org/10.1016/j.scitotenv.2021.147412, 2021.

Chen, Q., Li, J., Hua, X., Jiang, X., Mu, Z., Wang, M., Wang, J., Shan, M., Yang, X., Fan, X., Song, J., Wang, Y., Guan, D., and Du, L.: Identification of species and sources of atmospheric chromophores by fluorescence excitation-emission matrix with parallel factor analysis, Sci. Total Environ., 718, 137322, https://doi.org/10.1016/j.scitotenv.2020.137322, 2020.

Li, H., Zhang, Q., Jiang, W., Collier, S., Sun, Y., Zhang, Q., and He, K.: Characteristics and sources of water-soluble organic aerosol in a heavily polluted environment in Northern China, Sci Total Environ, 758, 143970, 10.1016/j.scitotenv.2020.143970, 2021.

Tang, J., Li, J., Su, T., Han, Y., Mo, Y., Jiang, H., Cui, M., Jiang, B., Chen, Y., Tang, J., Song, J., Peng, P. a., and Zhang, G.: Molecular compositions and optical properties of dissolved brown carbon in biomass burning, coal combustion, and vehicle emission aerosols illuminated by excitation–emission matrix spectroscopy and Fourier transform ion cyclotron resonance mass spectrometry analysis, Atmos. Chem. Phys., 20, 2513-2532, https://doi.org/10.5194/acp-20-2513-2020, 2020.

Yan, G. and Kim, G.: Speciation and Sources of Brown Carbon in Precipitation at Seoul, Korea: Insights from Excitation-Emission Matrix Spectroscopy and Carbon Isotopic Analysis, Environ. Sci. Technol., 51, 11580-11587, https://doi.org/10.1021/acs.est.7b02892, 2017.